BAI1 regulates spatial learning and synaptic plasticity in the hippocampus

Dan Zhu,[1] Chenchen Li,[2,3] Andrew M. Swanson,[3,4] Rosa M. Villalba,[3] Jidong Guo,[2,3] Zhaobin Zhang,[1] Shannon Matheny,[1] Tatsuro Murakami,[5,6] Jason R. Stephenson,[7] Sarah Daniel,[2,3] Masaki Fukata,[5,6] Randy A. Hall,[7] Jeffrey J. Olson,[1] Gretchen N. Neigh,[2,8] Yoland Smith,[3,9] Donald G. Rainnie,[2,3] and Erwin G. Van Meir[1]

[1]Laboratory of Molecular Neuro-Oncology, Departments of Neurosurgery and Hematology and Medical Oncology, School of Medicine and Winship Cancer Institute, Emory University, Atlanta, Georgia, USA. [2]Department of Psychiatry, Emory University School of Medicine, Atlanta, Georgia, USA. [3]Yerkes National Primate Research Center, Division of Behavioral Neuroscience and Psychiatric Disorders, Atlanta, Georgia, USA. [4]Neuroscience Graduate Program, Emory University, Atlanta, Georgia, USA. [5]Division of Membrane Physiology, Department of Cell Physiology, National Institute for Physiological Sciences, National Institutes of Natural Sciences, Okazaki, Japan. [6]Department of Physiological Sciences, School of Life Science, The Graduate University for Advanced Studies (SOKENDAI), Okazaki, Japan. [7]Department of Pharmacology, [8]Department of Physiology, and [9]Department of Neurology, Emory University School of Medicine, Atlanta, Georgia, USA.

Synaptic plasticity is the ability of synapses to modulate the strength of neuronal connections; however, the molecular factors that regulate this feature are incompletely understood. Here, we demonstrated that mice lacking brain-specific angiogenesis inhibitor 1 (BAI1) have severe deficits in hippocampus-dependent spatial learning and memory that are accompanied by enhanced long-term potentiation (LTP), impaired long-term depression (LTD), and a thinning of the postsynaptic density (PSD) at hippocampal synapses. We showed that compared with WT animals, mice lacking *Bai1* exhibit reduced protein levels of the canonical PSD component PSD-95 in the brain, which stems from protein destabilization. We determined that BAI1 prevents PSD-95 polyubiquitination and degradation through an interaction with murine double minute 2 (MDM2), the E3 ubiquitin ligase that regulates PSD-95 stability. Restoration of PSD-95 expression in hippocampal neurons in BAI1-deficient mice by viral gene therapy was sufficient to compensate for *Bai1* loss and rescued deficits in synaptic plasticity. Together, our results reveal that interaction of BAI1 with MDM2 in the brain modulates PSD-95 levels and thereby regulates synaptic plasticity. Moreover, these results suggest that targeting this pathway has therapeutic potential for a variety of neurological disorders.

Introduction

Synaptic plasticity refers to the ability of synapses to modify the strength or efficacy of synaptic transmission and is thought to underlie learning and memory (1, 2). Long-term potentiation (LTP) and long-term depression (LTD) are the most widely studied types of synaptic plasticity (3, 4), and their molecular mechanisms have been extensively explored in recent years (5–8). In the CA1 region of the hippocampus, it is well established that triggering of LTP requires synaptic activation of postsynaptic NMDA receptors (NMDARs) and subsequent downstream signaling cascades. While extensive progress has been made, much remains unknown about the identity and functional role of the specific proteins involved. Obtaining a better understanding of synaptic plasticity at the cellular and behavioral levels is particularly important, as such knowledge is crucial to developing novel diagnostics and therapeutics for multiple neurological disorders.

Brain-specific angiogenesis inhibitor 1 (BAI1) was recently identified as a postsynaptic density (PSD) protein (9, 10). BAI1 is a member of the adhesion GPCR subfamily (11), initially identified in a screen for p53-regulated genes (12). BAI1 is highly expressed in the normal brain but is epigenetically silenced in glioblastoma (12–15). BAI1 has been shown to exert potent antiangiogenic and antitumorigenic effects (16–18), and its loss or mutation in several cancers suggests that it is a tumor suppressor (19). BAI1 contains several well-defined protein modules in the N terminus such as an integrin-binding Arg-Gly-Asp (RGD) motif, followed by 5 thrombospondin type 1 repeats (TSRs), a hormone-binding domain, and a GPCR proteolytic cleavage site (GPS) (19). TSRs in BAI1 can regulate angiogenesis (12, 18, 20) and phagocytosis of apoptotic cells by macrophages (21) and participate in myogenesis (22). In the C terminus, BAI1 possesses a proline-rich region and a Gln-Thr-Glu-Val (QTEV) PDZ–binding motif, both of which are involved in protein-protein interactions (19).

Despite these recent advances, the pivotal role BAI1 plays in the CNS remains to be identified. Here, we generated a line of *Bai1*$^{-/-}$ (KO) mice to shed light on the physiological importance of BAI1 in the brain. The mutant mice were viable, with normal brain anatomy; however, behavioral testing revealed severe deficits in hippocampus-dependent spatial learning and memory, accompanied by abnormal synaptic plasticity. We provide evidence that the deficiency resulted from loss of a novel negative regulation of BAI1 upon MDM2, a ubiquitin ligase that targets PSD-95 for proteosomal degradation. Importantly, the synaptic plasticity deficits were reversible through PSD-95 gene therapy in the *Bai1*$^{-/-}$ hippocampus. We believe our findings uncover a previously unknown function of BAI1 in the brain, one that provides novel insights into syn-

Conflict of interest: The authors have declared that no conflict of interest exists.
Submitted: December 4, 2013; **Accepted:** January 15, 2015.
Reference information: *J Clin Invest*. 2015;125(4):1497–1508. doi:10.1172/JCI74603.

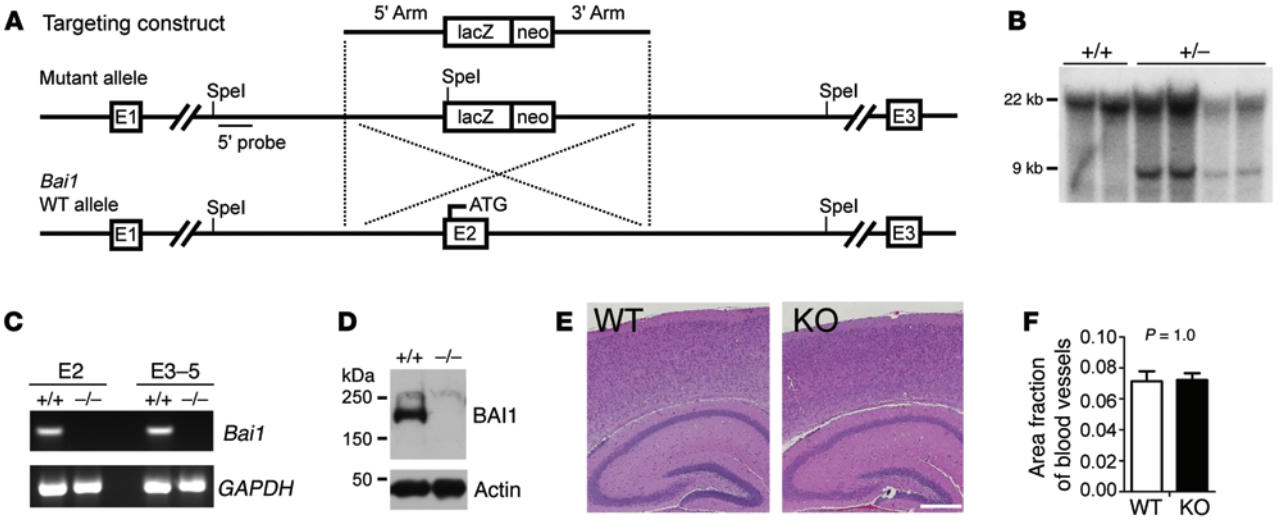

Figure 1. Generation and characterization of *Bai1*$^{-/-}$ mice. (**A**) Schematic of the *Bai1* gene–targeting strategy. Homologous recombination of the targeting construct with the mouse *Bai1* locus results in deletion of exon 2 (E2), which leads to a null mutation. (**B**) Southern blot genotyping of targeted ES cell clones. Genomic DNA from G418-resistant clones was digested with SpeI. After electrophoresis, the digested DNA was transferred to membrane and hybridized with the 5′ probe. The WT allele migrated as a 22-kb fragment, while the correct homologous recombinant allele migrated as a 9-kb fragment. (**C**) RT-PCR for *Bai1* gene transcripts from either exon 2 (E2) or exons 3–5 (E3–5) in 2-week-old WT and KO brains. (**D**) WB analysis to confirm the absence of BAI1 protein in homozygous KO ($^{-/-}$) mouse brains. (**E**) H&E staining of brain sections showed no apparent structural defects. Scale bar: 0.5 mm. (**F**) Quantification of vasculature in the brain showed no difference between WT and KO mice (n = 6 mice/group; P = 1.0 by 2-tailed Student's t test).

aptic plasticity and has therapeutic implications for a wide range of brain disorders.

Results

Generation and characterization of Bai1$^{-/-}$ *mice*. To generate a line of *Bai1*$^{-/-}$ mice, homologous recombination was used to target the *Bai1* gene in embryonic stem (ES) cells by replacement of exon 2 (where the start codon ATG is located) with a promoterless β-gal cDNA (*LacZ*) and a mini-neomycin resistance gene followed by a stop codon and poly-A tail (Figure 1A). Properly targeted G418-resistant clones were confirmed by Southern blotting (Figure 1B), and 2 independent clones with normal karyotypes, morphology, and growth rate were injected into C57BL/6 blastocysts to achieve germline transmission. Once the *Bai1*$^{-/-}$ mice were generated, we confirmed the absence of *Bai1* gene expression (Figure 1C) and protein expression (Figure 1D). The results from the 2 lines were identical, thus we did not document the lines separately in the data described below. The *Bai1*$^{-/-}$ mice were viable and fertile and obtained at the expected Mendelian ratio (Supplemental Figure 1; supplemental material available online with this article; doi:10.1172/JCI74603DS1), without obvious anatomical abnormalities, including in the brain (Figure 1E). Since BAI1 is a negative regulator of angiogenesis (14), we examined the *Bai1*$^{-/-}$ brain vasculature thoroughly, but found no defects (Figure 1F). Moreover, we did not observe any brain tumors in the *Bai1*$^{-/-}$ mice for at least 1.5 years, suggesting that deletion of the tumor-suppressive activity of BAI1 per se is not sufficient to initiate brain tumor formation in mice.

Bai1$^{-/-}$ *mice show deficits in hippocampus-dependent learning and memory*. To identify any potential defective phenotype, we first performed behavioral tests using *Bai1*$^{-/-}$ and WT littermate mice to evaluate the effect of *Bai1* loss on behavior. BAI1 is abundant in the hippocampus (15, 23), a key region for spatial learning and memory. Thus, we tested these cognitive functions by performing a hidden-platform version of the Morris water maze task (24), which is hippocampus- and NMDAR dependent (25). Mice were trained to find a submerged hidden platform using spatial cues (acquisition), after which the platform was removed to test memory retention (probe trial). WT mice showed a progressive reduction in their escape latency over the period of acquisition, as the slope of the learning curve was significantly steeper for WT mice than it was for *Bai1*$^{-/-}$ mice, indicating that the *Bai1*$^{-/-}$ mice were deficient in learning this task (Figure 2A). On day 6, a probe trial was performed, and the time spent in each quadrant was quantified. Notably, the *Bai1*$^{-/-}$ mice did not show a preference for the target quadrant, whereas the WT mice spent significantly more time in the target quadrant (Figure 2B), suggesting impairment in spatial learning and memory in *Bai1*$^{-/-}$ mice. As a control, we repeated the test with a visible platform and detected no differences between the *Bai1*$^{-/-}$ and WT mice (Figure 2, C and D). These data exclude concealed defects in the noncognitive skills needed to complete the test, including visual acuity and motor skills for swimming and mounting the platform. Moreover, we observed no significant differences in anxiety-like behavior as assessed in the elevated plus maze (Figure 2E), the marble-burying test (Figure 2F), and the light/dark test (Figure 2G). Collectively, these results reveal that *Bai1*$^{-/-}$ mice have severely impaired spatial learning and memory, yet display normal motor function and anxiety-like behavior.

Bai1$^{-/-}$ *mice display major changes in frequency-dependent synaptic plasticity*. To determine whether the impaired spatial learning and memory of *Bai1*$^{-/-}$ mice might be related to alterations in synaptic plasticity in the hippocampus, we assessed the effects of *Bai1* loss on NMDAR-dependent LTP and LTD induction in CA1 pyramidal neurons ex vivo. To ensure that any observed changes

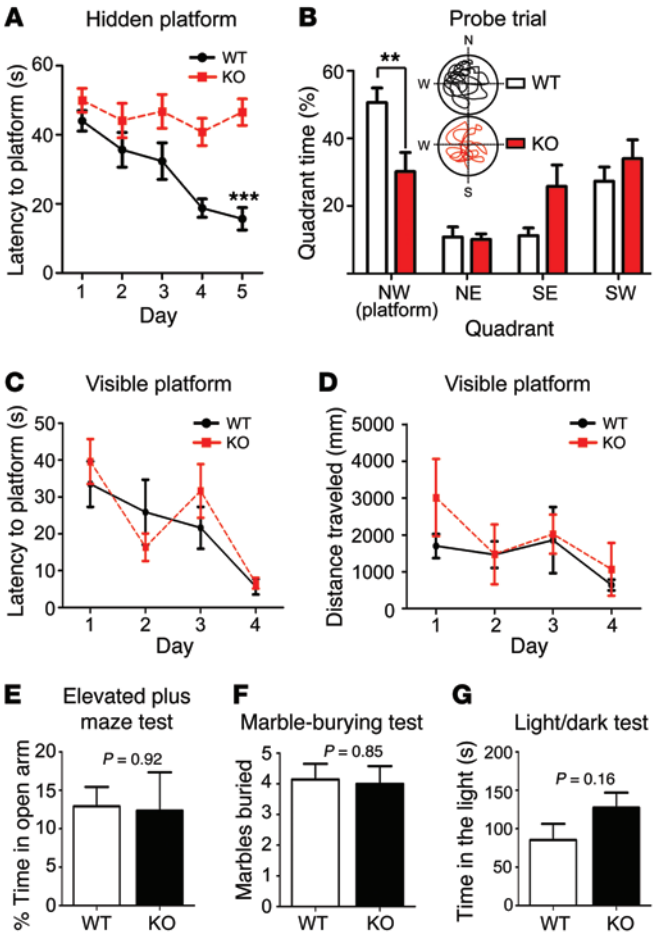

Figure 2. *Bai1*$^{-/-}$ mice show deficits in hippocampus-dependent learning and memory. (**A**) Escape latency curve during hidden-platform Morris water maze acquisition showed that WT mice improved substantially, while KO mice did not (n = 10 mice/group; ***P < 0.001 by 2-way ANOVA with Dunnett's post-hoc test). (**B**) Quantification of time spent in each quadrant during probe trials with representative swimming paths of WT and KO mice. WT mice showed a significant preference for the northwest (NW) target quadrant (n = 10 mice/group; **P < 0.01 by 2-way ANOVA with Dunnett's post-hoc test). Escape latencies (**C**) and distance traveled (**D**) during the visible-platform Morris water maze test. No significant differences were detected between WT and KO mice (n = 8 mice/group; P = 0.64 and P = 0.32, respectively, by 2-way ANOVA). Anxiety-like behavior was assessed by the elevated plus-maze test (n = 8 mice/group; P = 0.92 by 2-tailed Student's t test) (**E**); the marble-burying test (7 mice/group; P = 0.85 by 2-tailed Student's t test) (**F**); and the light/dark test (n = 8 mice/group; P = 0.16 by 2-tailed Student's t test) (**G**). There was no significant difference between WT and KO mice. All data represent the mean ± SEM.

in synaptic plasticity were dependent on the frequency of stimulation, we first examined hippocampal basal excitatory synaptic transmission at Schaffer collateral synapses and found no significant changes in the *Bai1*$^{-/-}$ mice (Supplemental Table 1). We then investigated whether a spaced high-frequency stimulation (HFS) of the Schaffer collateral input might show differences in LTP induction in CA1 neurons. HFS induced a robust enhancement in excitatory postsynaptic currents (EPSCs) that lasted for more than 40 minutes in WT and *Bai1*$^{-/-}$ mice (Figure 3A). However, while the initial LTP was similar for both types of mice and reached steady state in WT neurons (1.75 ± 0.24 fold over baseline, 30 minutes after HFS, n = 8 neurons from 6 animals), the magnitude of LTP continued to increase in the *Bai1*$^{-/-}$ mice, showing significant enhancement (2.85 ± 0.29 fold over baseline, 30 minutes after HFS, n = 6 neurons from 4 animals, P < 0.001) (Figure 3A). We next examined the effects of *Bai1* deletion on LTD using a low-frequency stimulation (LFS) protocol (1 Hz), which normally induces stable LTD in slices from WT mice (0.67 ± 0.10 fold over baseline, n = 6 neurons from 3 animals) (Figure 3B). Intriguingly, LFS failed to induce LTD in *Bai1*$^{-/-}$ slices, but rather induced significant LTP (1.41 ± 0.07 fold, n = 5 neurons from 3 animals) (Figure 3B). These studies revealed enhanced LTP and an apparent loss of LTD at *Bai1*$^{-/-}$ hippocampal CA1 synapses. Similar results were obtained with stimulation frequencies of 5 Hz and 10 Hz, respectively (Figure 3, C and D). Taken together, these results indicate that the frequency dependence of synaptic plasticity was dramatically altered in *Bai1*$^{-/-}$ CA1 pyramidal neurons (Figure 3E). To determine any potential effects on presynaptic release, we also examined the paired-pulse ratio (PPR) of evoked EPSCs (eEPSCs), a measure of short-term presynaptic plasticity. No significant PPR differences were detected between WT and *Bai1*$^{-/-}$ slices (Figure 3F), suggesting that the observed alterations in synaptic plasticity were primarily postsynaptic.

Bai1$^{-/-}$ *hippocampal CA1 neurons have normal dendritic arborization and spine density*. Synaptic plasticity can be associated with changes in dendritic spine morphology (26). A recent in vitro study suggested that BAI1 interaction with the PAR3/TIAM1 polarity complex regulates spinogenesis in neurons in culture (10). Therefore, we examined whether the aberrant synaptic plasticity in *Bai1*$^{-/-}$ mice correlated with alterations in dendritic spine morphology in ex vivo *Bai1*$^{-/-}$ hippocampus. The spines in hippocampal slices were visualized by filling individual CA1 pyramidal neurons with biocytin. The overall morphology of adult *Bai1*$^{-/-}$ hippocampal CA1 neurons had no apparent defects in either the numbers of primary dendrites or the dendritic branches (Figure 4A). Dendritic protrusions on basal, proximal, and distal apical dendrites were classified into different spine categories (stubby, mushroom, or thin) (27) (Figure 4B) and quantified. Compared with WT neurons, neither the proportion nor the total number of dendritic spines was significantly changed in *Bai1*$^{-/-}$ neurons (Figure 4, C and D). To determine whether deletion of *Bai1* in mice has any effect on spinogenesis or synaptogenesis, we also examined dendritic spine morphology during early postnatal development (3 weeks old) and detected no significant alterations in spine density or spine category proportion (Supplemental Figure 2). Taken together, these results suggest that the *Bai1*$^{-/-}$ hippocampal CA1 pyramidal neurons display no significant structural changes in dendritic arborization or spine formation and/or maturation when examined at the light microscopic level.

Bai1$^{-/-}$ *hippocampal CA1 neurons have decreased PSD thickness*. We further examined the synaptic ultrastructure by electron microscopy. Altogether, 227 PSDs at the hippocampal CA1 stratum radiatum were randomly sampled in a blind analysis. Consistently, we found no significant changes in spine density or spine size (data not shown), but interestingly, we observed an approximately 40% reduction in the thickness of PSD regions in *Bai1*$^{-/-}$

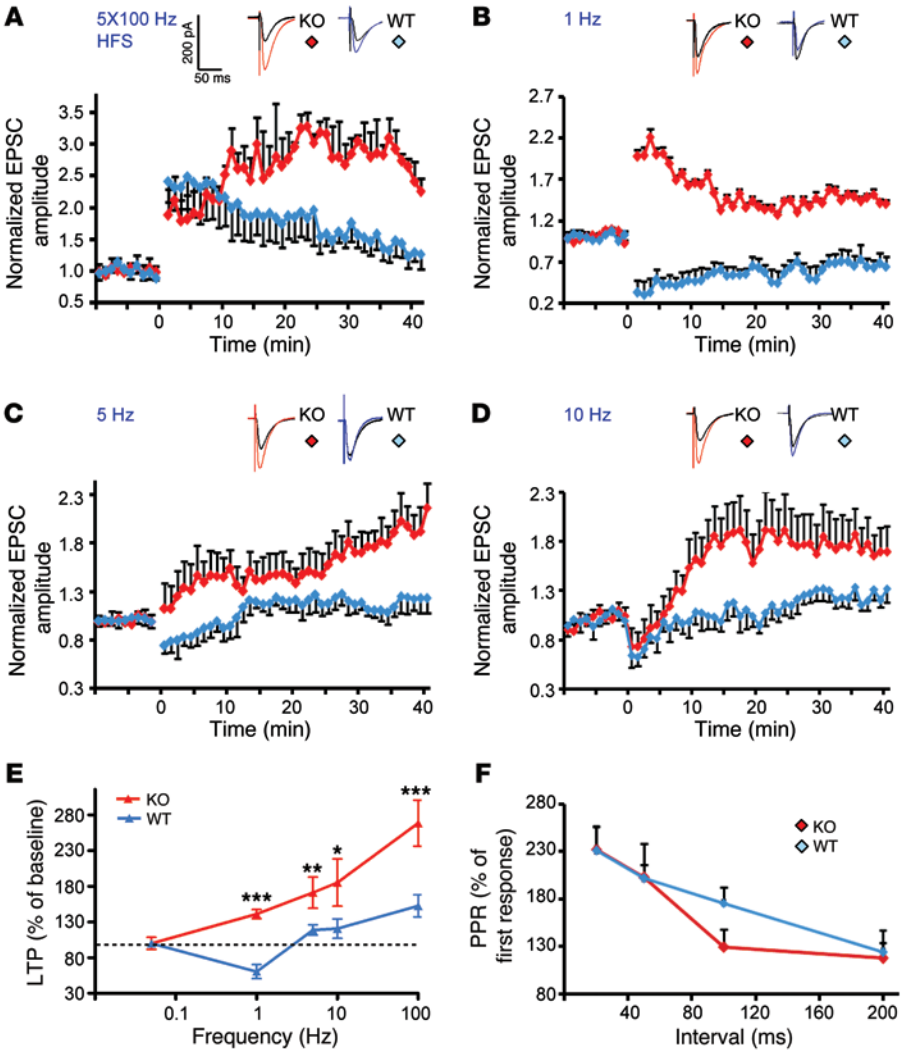

Figure 3. *Bai1*$^{-/-}$ mice display changes in frequency-dependent synaptic plasticity. (**A**) HFS-induced LTP was elicited using 5 × 100 Hz trains of stimulation at 20-second intervals. Note the enhanced potentiation after HFS stimulation in slices from KO mice (red) compared with slices from WT mice (blue) (6 mice/WT group, 4 mice/KO group; $P < 0.001$). (**B**) Stimulation (900 pulses) delivered at 1 Hz induced LTD in slices from WT mice (blue), but conversely induced robust LTP in KO mice (red) ($n = 3$ mice/group; $P < 0.001$). (**C**) Stimulation (900 pulses) was delivered at either 5 Hz or 10 Hz (**D**). Note that both stimulation protocols induced enhanced LTP in slices from KO animals (red) (4 mice/WT group, 3 mice/KO group; $P < 0.05$ and $P < 0.01$, respectively). (**E**) Summary of the ability of different frequencies of stimulation to induce changes in synaptic strength in hippocampi of WT (blue) and KO mice (red) mice. ***$P < 0.001$; **$P < 0.01$; *$P < 0.05$. (**F**) PPR was measured using pairs of presynaptic stimulation pulses separated by 20, 50, 100, and 200 ms. All data represent the mean ± SEM and were analyzed using the 2-tailed Student's *t* test.

neurons compared with those in WT neurons (30.5 ± 0.7 nm for WT vs. 18.7 ± 0.5 nm for *Bai1*$^{-/-}$, $P < 0.001$) (Figure 5). A similar reduction was also observed during early postnatal development (3 weeks old) and in cortex somatosensory neurons (Supplemental Figure 3). These results suggest that *Bai1*$^{-/-}$ CA1 neurons have defects in their excitatory synaptic ultrastructural architecture.

PSD-95 protein levels are reduced in the Bai1$^{-/-}$ *brain.* The PSD is an electron-dense thickening in the postsynaptic membrane that is composed of a protein network including various receptors, ion channels, adhesion molecules, scaffolding proteins, cytoskeletal proteins, and associated signaling molecules (28, 29). PSD-95, the most abundant scaffolding protein in the PSD (30), is critical for excitatory synapse formation, maturation, and function (31, 32). A recent study suggested that PSD-95 is required to sustain the molecular organization of the PSD, and RNA interference knockdown of PSD-95 leads to a breakup or shortening of the PSD (33). Hence, we hypothesized that the decrease in PSD thickness in our *Bai1*$^{-/-}$ mice was due to perturbations of PSD-95. To test this, we first determined PSD-95 protein levels by Western blot (WB) analysis and found a remarkable reduction (~50%) in these levels in *Bai1*$^{-/-}$ brain (Figure 6A). This reduction was specific to PSD-95, since the expression levels of 2 other postsynaptic proteins, NMDAR NR1 subunit (NMDAR1) and calmodulin-dependent protein kinase II (CaMKII), remained unchanged. The reduction was not region specific, as we observed a similar decrease in PSD-95 levels in neocortex, hippocampus, and cerebellum (Figure 6B). In contrast, the protein levels of BAI1-associated protein 2 (BAIAP2) were not altered. We hypothesized that the reduction in total PSD-95 protein levels results predominantly from decreases in the synaptic pool of PSD-95. Consistent with this idea, examination of PSD-95 levels in purified PSD fractions revealed a substantial reduction in the postsynaptic compartment (Figure 6C). Taken together, these findings indicate a remarkable reduction of PSD-95 protein at *Bai1*$^{-/-}$ synapses. We next explored the mechanisms underlying this reduction. No decreases in *PSD-95* mRNA levels were detected (Figure 6D), revealing that transcriptional suppression could not account for the decrease in protein levels. To test whether PSD-95 stability is changed in *Bai1*$^{-/-}$ synapses, DIV12 high-density cortical neuron cultures were treated with cycloheximide (CHX), a protein synthesis blocker, and the kinetics of protein degradation were compared between WT and *Bai1*$^{-/-}$ neurons (Figure 6E). Remarkably, after 8 hours of protein synthesis inhibition, 49% ± 4% of PSD-95 protein remained in WT neurons, while only 24% ± 3% remained in *Bai1*$^{-/-}$ neurons. The degradation rate of PSD-95 was approximately

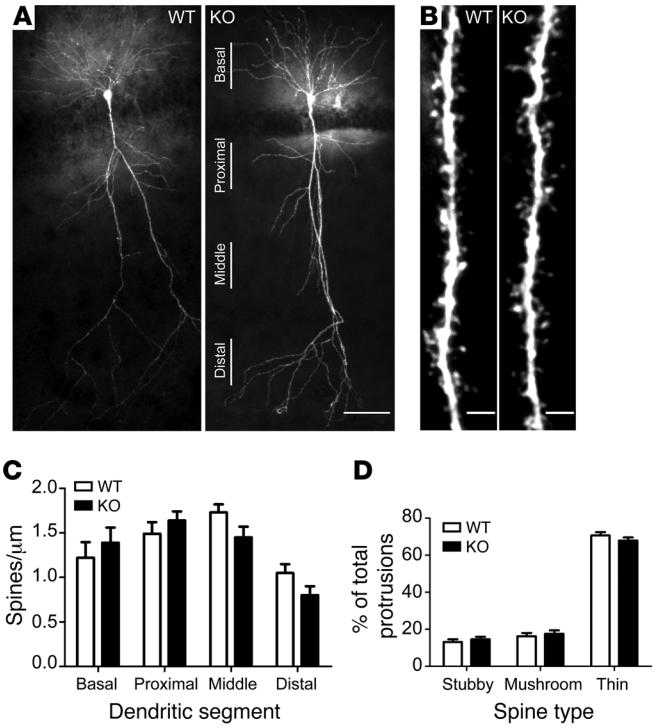

Figure 4. *Bai1*$^{-/-}$ hippocampal CA1 neurons have normal dendritic arborization and spine morphology. (**A**) Representative images of biocytin-filled CA1 neurons from adult WT and KO mice show normal dendritic arborization in KO mice. Scale bar: 50 μm. (**B**) Representative images from apical segments of WT and KO neurons show unaffected dendritic spine density and morphology. Scale bars: 2 μm. (**C**) No significant difference in dendritic spine density was observed between WT and KO CA1 neurons. Secondary dendritic segments were captured from basal dendrites, proximal apical dendrites (50–100 μm from the soma), middle apical dendrites (100–150 μm from the soma), and distal apical dendrites (>150 μm from the soma). n = 5 mice/group; P = 0.55. (**D**) Dendritic spine morphology was not affected in KO neurons. Spines were classified as stubby, mushroom, or thin and were quantified. n = 5 mice/group; P = 0.99. All data represent the mean ± SEM and were analyzed by 2-way ANOVA.

2-fold faster in *Bai1*$^{-/-}$ neurons than in WT neurons, suggesting that loss of *Bai1* promotes PSD-95 degradation.

Association of BAI1 with MDM2 inhibits PSD-95 polyubiquitination and degradation. PSD-95 degradation is regulated by the proteasome and involves the E3 ubiquitin ligase MDM2 (34). Our finding that PSD-95 degradation is enhanced in *Bai1*$^{-/-}$ brain suggested a novel function for BAI1 as a negative regulator of MDM2-mediated PSD-95 ubiquitination. To test this hypothesis, we transiently transfected mammalian cells with expression vectors for PSD-95, HA-tagged ubiquitin, BAI1, and MDM2. Cotransfection with BAI1 induced a striking stabilization of PSD-95 levels, accompanied by a substantial reduction in high-molecular-weight polyubiquitinated PSD-95 (Figure 7A). The inhibitory effect was evident, even in the presence of MDM2 overexpression. One possible mechanism for this inhibitory effect is that BAI1 binds to PSD-95 and prevents its polyubiquitination by MDM2, through either competitive or allosteric inhibition. To test this, we used a BAI1-mutant construct that lacks the QTEV PDZ–binding motif. Deletion of the QTEV motif blocked the interaction between BAI1 and PSD-95; however, this mutant retained the ability to inhibit PSD-95 polyubiquitination and stabilized PSD-95 (Figure 7B), suggesting that the interaction of BAI1 with PSD-95 is not required for BAI1-mediated stabilization of PSD-95. As an alternative hypothesis, we postulated that BAI1 interferes with MDM2 function through direct MDM2 binding. Coimmunoprecipitation (Co-IP) experiments on mouse brain tissue extracts revealed a novel in vivo interaction between BAI1 and MDM2 (Figure 7C). To further characterize the MDM2 protein domains involved, we transiently cotransfected BAI1 with MDM2 WT and mutant constructs (35) in 293FT cells, which lack endogenous PSD-95 expression. Deletion of aa 1–200 from MDM2 blocked the interaction with BAI1, deletion of aa 200–300 markedly attenuated it, and deletion of aa 300–491 had no effect (Figure 7D). To further define the importance of the BAI1-MDM2 interaction for PSD-95 stability and to confirm the role of the N terminus of MDM2 in binding, we repeated the cotransfection in the presence of an HA-tagged MDM2 fragment (aa 1–215) expression vector. We hypothesized that this fragment blocks the BAI1-MDM2 (WT) interaction in a dominant-negative fashion. Overexpression of the MDM2 fragment did inhibit the interaction between BAI1 and the full-length Myc-tagged MDM2 (Figure 7E, left panel), resulting in enhanced polyubiquitination of PSD-95 and a substantial reduction of PSD-95 protein levels (Figure 7E, right panel). These results show that the BAI1-MDM2 interaction inhibits PSD-

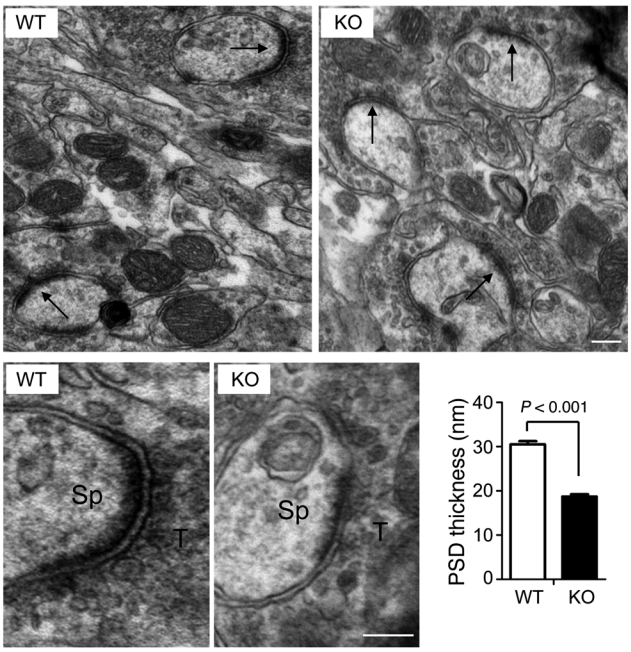

Figure 5. Decrease in PSD thickness in *Bai1*$^{-/-}$ hippocampal neurons by electron microscopic analysis. Top: Representative electron micrographic images of asymmetric axospinous synapses (arrows) in the CA1 region of adult WT and KO mice. Bottom: High-magnification images showing individual synapses. Sp, spine; T, axon terminal. Scale bars: 100 nm. Histogram shows the significant difference in the mean ± SEM of PSD thickness between WT and KO animals (n = 5 mice/group; P < 0.001 by 2-tailed Student's t test).

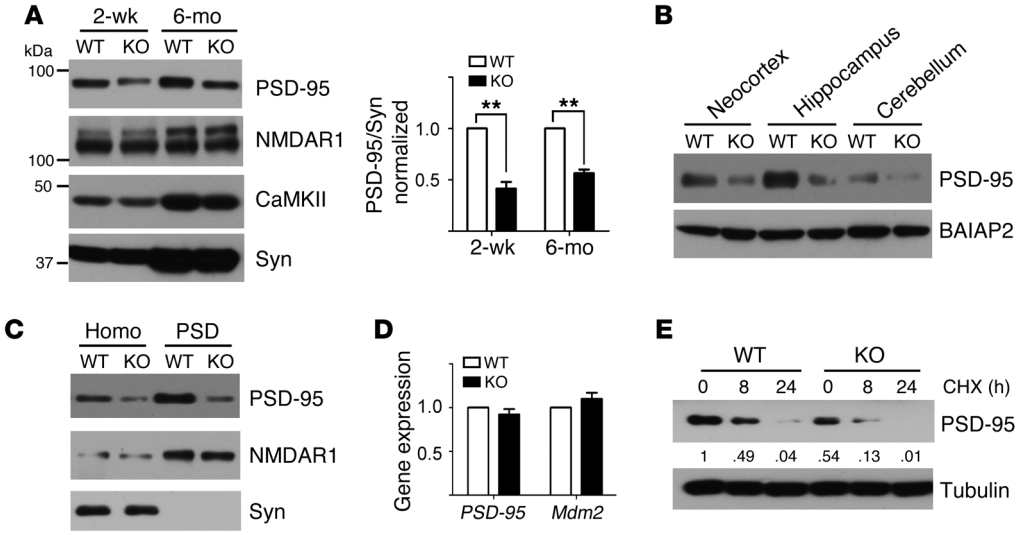

Figure 6. *Bai1*$^{-/-}$ mice have reduced PSD-95 protein levels. (**A**) PSD-95 protein levels were reduced by approximately 50% in brains of 2-week-old pups and 6-month-old adult KO mice, while expression levels of NMDAR1, CaMKII, and presynaptic marker synaptophysin (Syn) remained unchanged. Blots shown are from samples that were run in parallel. Quantification of PSD-95 is shown on the right (n = 6; $^{**}P < 0.01$ by 2-tailed Student's t test). (**B**) WB showing that PSD-95 protein levels were reduced in neocortex, hippocampus, and cerebellum of adult mice, while BAIAP2 expression levels remained unchanged. (**C**) Substantial reduction of PSD-95 in the PSD fraction of adult KO mice. Homo, cell homogenate. (**D**) Quantitative RT-PCR showed that *PSD-95* mRNA levels were not reduced in KO mice. (**E**) PSD-95 was more rapidly degraded in cultured primary cortical neurons from KO mice. CHX (30 μg/ml) was added to block de novo protein translation in high-density dissociated cortical neurons for 0, 8, and 24 hours. Cell lysates were collected and subjected to WB analysis. Relative band intensities are indicated. All histograms show the mean ± SEM. All blots show representative images from 3 independent experiments with similar results.

95 ubiquitination and stabilizes its protein levels in cell culture. To determine whether this regulation also occurs under physiological conditions in vivo, we examined PSD-95 ubiquitination and protein levels in WT and *Bai1*$^{-/-}$ mice. Consistent with our in vitro findings, we observed a greater than 2-fold increase in PSD-95 polyubiquitination in brain tissue from 2-week- and 6-month-old *Bai1*$^{-/-}$ mice (Figure 7F and Supplemental Figure 4), which was accompanied by an increased PSD-95–MDM2 association. BAI1 loss did not lead to a general destabilization of PSD proteins, as the levels of guanylate kinase–associated protein (GKAP), an abundant PSD protein that binds PSD-95 directly (36) and is regulated by the TRIM3 E3 ligase (37), remained unaffected (Supplemental Figure 4). Taken together, these cellular and in vivo approaches suggest that BAI1 can stabilize PSD-95 expression by preventing MDM2-mediated ubiquitination of PSD-95.

Restoration of PSD-95 expression in Bai1$^{-/-}$ *hippocampus rescues synaptic plasticity deficits*. To directly assess whether the reduction in PSD-95 levels might be the underlying cause of the aberrant synaptic plasticity elicited by the loss of *Bai1*, we restored PSD-95 expression in the *Bai1*$^{-/-}$ hippocampus of 6- to 8-week-old mice. For this purpose, we generated novel adeno-associated viruses (AAVs) coexpressing GFP and PSD-95 via an F2A motif (ref. 38 and Figure 8A). Since palmitoylation of the N terminus of PSD-95 is critical for its synaptic localization and function (39), we confirmed that the PSD-95 expressed from our expression vector can be efficiently palmitoylated using an in vitro assay (ref. 40 and Supplemental Figure 5). The AAVs were then locally infused into the dorsal hippocampus through stereotactic neurosurgery (Figure 8B). Four to five weeks after infection, we detected strong GFP expression in hippocampal CA1, and WB analysis confirmed restoration of PSD-95 protein expression (Figure 8B). Remarkably, restoration of PSD-95 protein expression in *Bai1*$^{-/-}$ neurons was sufficient to prevent abnormal LTP induction at different frequencies of synaptic stimulation (Figure 8C and Supplemental Figure 6). Patch-clamp recordings in PSD-95–restored *Bai1*$^{-/-}$ neurons 4–5 weeks after infection revealed WT-like LTD in response to a 1-Hz stimulation (0.55 ± 0.09 fold over baseline), while *Bai1*$^{-/-}$ neurons infected with the control GFP virus still exhibited aberrantly enhanced LTP (1.50 ± 0.10 fold over baseline, 1 Hz; 1.66 ± 0.21 fold over baseline, 5 Hz). Taken together, these results demonstrate that restoration of PSD-95 in the *Bai1*$^{-/-}$ hippocampus was sufficient to restore normal synaptic plasticity. To further assess the possibility of a direct cause-effect relationship between the BAI1-MDM2 interaction, PSD-95 stability, and hippocampal synaptic plasticity, we took advantage of our MDM2 dominant-negative fragment (aa 1–215). Overexpression of this fragment blocked the MDM2-BAI1 interaction in transfected mammalian cells and resulted in enhanced PSD-95 degradation (Figure 7E). Thus, we hypothesized that in vivo overexpression of this fragment should mimic, at least in part, the deficits observed in *Bai1*$^{-/-}$ neurons. To test this, we designed an AAV expression vector for the MDM2 (aa 1–215) fragment and first confirmed its destabilizing effects on endogenous PSD-95 stability in primary neuronal cell cultures (Supplemental Figure 7). We then injected it into the WT mouse hippocampus. Strikingly, patch-clamp recordings in the infected neurons antagonized LTD induction in response to the 1-Hz stimulation (1.03 ± 0.27 fold over baseline, n = 7 neurons from 6 animals; $P < 0.001$, Student's t test) (Figure 8D). Taken together, these results demonstrate that blocking the interaction between BAI1 and MDM2 in WT hippocampal neu-

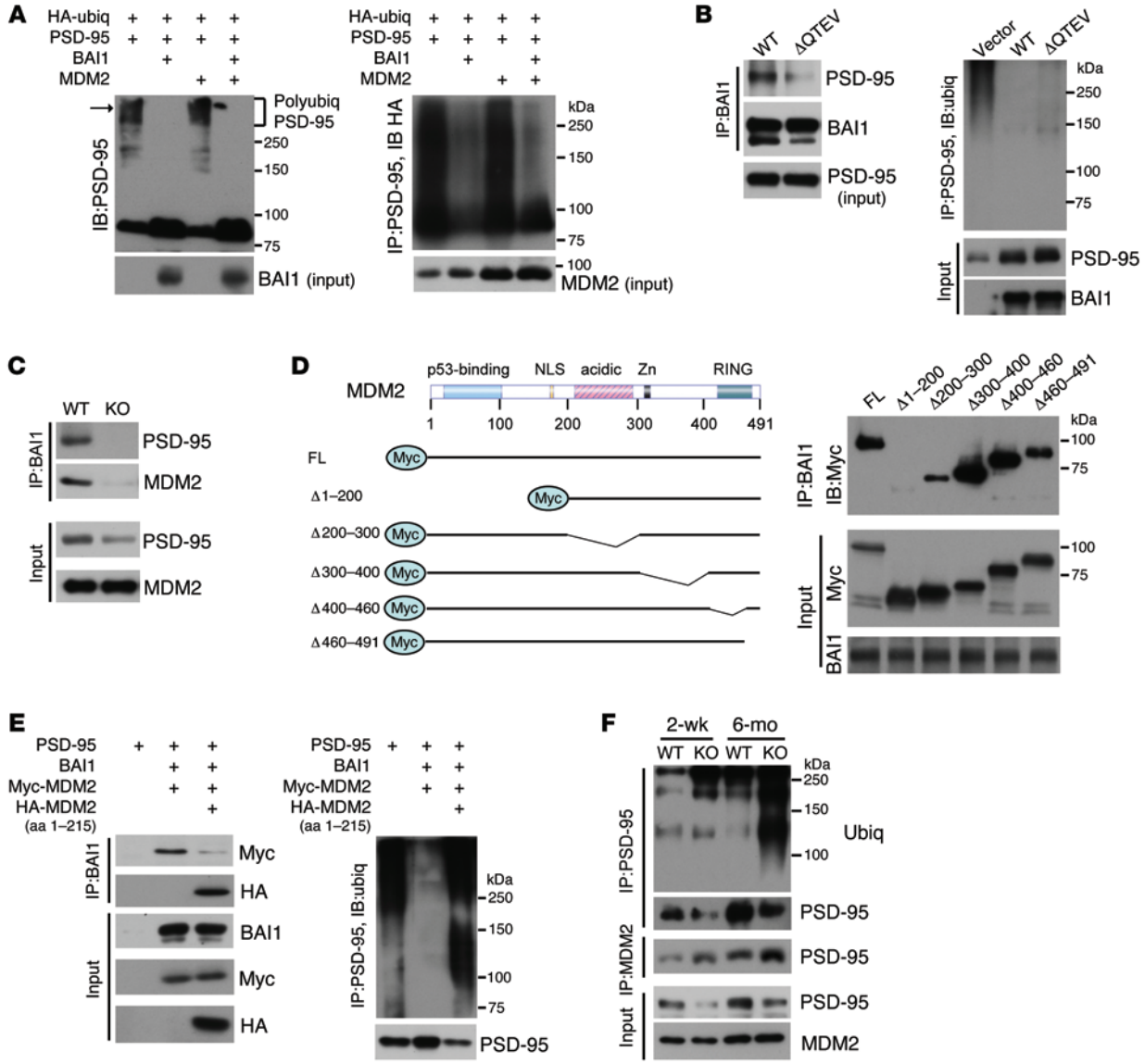

Figure 7. BAI1 binds MDM2 and prevents PSD-95 polyubiquitination. (**A**) BAI1 attenuated PSD-95 polyubiquitination. HEK 293FT cells were transiently transfected with the indicated expression vectors. Left panel: Immunoblot (IB) detected PSD-95 and high-molecular-weight polyubiquitinated PSD-95 (arrow). Right panel: Co-IP with anti–PSD-95 antibody, followed by IB detection of ubiquitin chains (anti-HA antibody). (**B**) Deletion of the BAI1 QTEV motif blocked the BAI1–PSD-95 interaction (left panel), but retained the ability to inhibit PSD-95 polyubiquitination (right panel). HEK 293FT cells were transiently cotransfected with expression vectors for PSD-95 with either BAI1 WT or mutant plasmid. Antibodies used for Co-IP and IB are indicated. Blots shown are from samples that were run in parallel. (**C**) Co-IP shows the BAI1-MDM2 association in adult WT mouse brain. (**D**) Interaction of BAI1 and MDM2 in transfected HEK 293FT cells. Left: Schematic drawing of the full-length (FL) and truncated MDM2 constructs. Right: HEK 293FT cells were cotransfected with expression vectors for BAI1 and Myc-tagged full-length MDM2 or the indicated deletion mutants. (**E**) Overexpression of a dominant-negative MDM2 (HA-MDM2) blocked the BAI1-MDM2 (WT) interaction (left panel) and enhanced PSD-95 polyubiquitination (right panel). HEK 293FT cells were transiently transfected with the indicated expression vectors. Myc-MDM2, full-length Myc-tagged MDM2; HA-MDM2, HA-tagged N terminus of MDM2 (aa 1–215). (**F**) Co-IP experiments on brain extracts from 2-week- and 6-month-old WT and KO mice showed increased polyubiquitination of PSD-95 and PSD-95–MDM2 interaction in KO mouse brains. All blots show representative images from 3 independent experiments with similar results.

rons is sufficient to prevent the induction of LTD, thereby mimicking the plasticity deficits observed in *Bai1*$^{-/-}$ mice.

Discussion

BAI1 has been primarily studied as a negative regulator of angiogenesis and tumorigenesis (19, 41). Surprisingly, we did not detect any vascular abnormalities in the *Bai1*$^{-/-}$ brain. We found no evidence for augmented tumor predisposition either, demonstrating that BAI1 loss is not a tumor-initiating event in C57BL/6 mice. Additional studies are needed to determine whether other proteins can compensate for the loss of the antiangiogenic function of BAI1 in *Bai1*$^{-/-}$ mice. Furthermore, crossing of *Bai1*$^{-/-}$ mice with strains predisposed to tumor formation will determine whether BAI1 loss can accelerate tumor progression.

BAI1 is highly expressed in neurons (42), yet its physiological function in the CNS remains elusive. Here, we uncover, for the first

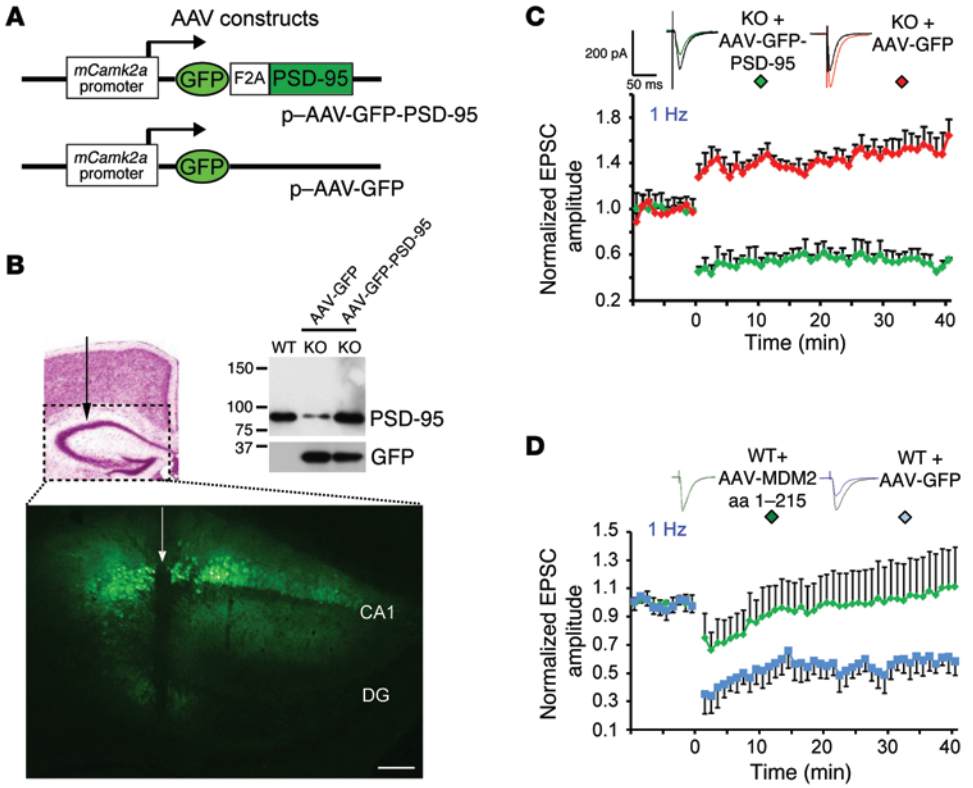

Figure 8. Restoration of PSD-95 expression in *Bai1*$^{-/-}$ hippocampal neurons rescues synaptic plasticity deficits. (**A**) Schematic of AAV expression vectors. A single *Camk2a* promoter–driven cistron that yielded separate GFP and PSD-95 protein expression through an F2A motif was engineered. (**B**) Four to five weeks after AAV injection into the dorsal side of the hippocampus, GFP could be readily detected (needle track indicated by an arrow). Scale bar: 100 μm. DG, dentate gyrus. WB analysis of hippocampal extracts shows restoration of PSD-95 protein levels (top panel). (**C**) Reversal of LTP following AAV-mediated restoration of PSD-95 expression in KO hippocampal neurons. In the 1-Hz stimulation protocol, enhanced LTP could only be detected in control GFP–infected KO neurons (red), whereas LTD was detected in PSD-95–AAV–infected KO neurons (green) (n = 3 mice/group. $P < 0.001$ by 2-tailed Student's t test). (**D**) Blockage of LTD following AAV-mediated disruption of BAI1-MDM2 interaction in WT hippocampal CA1 neurons. In the 1-Hz stimulation protocol, LTD could only be detected in control AAV–GFP–infected WT neurons (blue) (n = 6 mice/group. $P < 0.001$ by 2-tailed Student's t test).

time to our knowledge, an unappreciated function of BAI1 in the brain as a critical regulator of synaptic plasticity at hippocampal excitatory synapses. Indeed, our electrophysiological data reveal an important role for BAI1 in regulating NMDAR-dependent synaptic plasticity in vivo. In *Bai1*$^{-/-}$ CA1 neurons, both HFS and LFS induced a sharp enhancement of LTP, while the latter normally induces a stable LTD in WT slices. These results indicate that the frequency dependence of synaptic plasticity is dramatically altered in *Bai1*$^{-/-}$ CA1 pyramidal neurons. Since no significant changes were detected in paired-pulse facilitation (considered a presynaptic phenomenon) in *Bai1*$^{-/-}$ CA1 neurons, the alterations in synaptic plasticity in *Bai1*$^{-/-}$ hippocampus are most likely postsynaptic.

Consistent with the observed alterations in hippocampal CA1 synaptic plasticity, we detected spatial learning and memory deficits in *Bai1*$^{-/-}$ mice. In particular, *Bai1*$^{-/-}$ mice showed severe deficits in the hidden-platform water maze test, while performing normally in the visible-platform water maze test and several anxiety tests, suggesting that *Bai1* deficiency has specific effects on cognitive function. Traditionally, LTP has been designated as a primary mediator of spatial memory storage in the hippocampus, and enhancements in LTP are often positively correlated with learning (3, 43). However, we observed an inverse correlation, analogous to the findings reported for studies on mice lacking PSD-95 (44). Intriguingly, recent accumulating evidence supports the idea that LTP and LTD may enable distinct and separate forms of information storage, with LTD dominating in the processing of precise spatial characteristics (45). Thus, the impairment in LTD induction in *Bai1*$^{-/-}$ mice is likely to be highly relevant to the deregulated memory storage and learning deficits that we observed in the behavioral studies.

We then characterized the underlying mechanisms and first considered structural defects. The *Bai1*$^{-/-}$ mouse brain anatomy looked normal under light microscopy, the hippocampal CA1 pyramidal neurons showed normal dendritic arborization, and no significant changes in spine formation and/or maturation were detected. Similarly, neurons in the brains of *Baiap2*$^{-/-}$ mice exhibited perturbations of synaptic plasticity in the absence of changes in dendritic spine morphology (46, 47). However, further examination at the ultrastructural level evidenced a thinning of the PSD in *Bai1*$^{-/-}$ mice CA1 neurons by electron microscopy. This was accompanied by a remarkable decrease in the levels of PSD-95, a canonical PSD component that regulates synapse maturation and synaptic plasticity (44, 48). Importantly, restoration of PSD-95 in adult *Bai1*$^{-/-}$ mice hippocampi was able to rescue synaptic plasticity deficits, suggesting that the perturbed synaptic plasticity observed in *Bai1*$^{-/-}$ CA1 neurons is due in large part to the destabilization of PSD-95. These findings, along with the observation that *Bai1*$^{-/-}$ mice and *PSD-95*–mutant mice show strikingly similar phenotypes (enhanced LTP, reduced LTD, and deficits in spatial learning and memory), suggest that dysregulation of PSD-95 is the primary underlying cause of these deficits observed in *Bai1*$^{-/-}$ mice. These findings establish a novel functional relationship between BAI1 and PSD-95. Interestingly, some recent studies suggested that basal synaptic transmission is altered in the *PSD-95*–mutant mice (49, 50); however, we did not detect significant changes in spontaneous EPSPs in our *Bai1*$^{-/-}$ mice. These results suggest that the phenotypes of PSD-95 mutants and *Bai1*$^{-/-}$ mice are not exactly identical and that an approximately 50% reduction in PDS-95 dosage in the *Bai1*$^{-/-}$ mice may only impair part of the function of PSD-95, or that differences in compensatory mechanisms exist between the 2 types of mice.

PSD-95 associates with MDM2, an E3 ubiquitin ligase that mediates ubiquitination and degradation of PSD-95 and regulates the function of many cancer-related proteins (34, 51, 52). Here, for the first time to our knowledge, we demonstrate a novel protein-protein interaction between BAI1 and MDM2, which establishes BAI1 as a novel upstream regulator of the MDM2–PSD-95 interaction and possibly of other MDM2 targets, including the p53 and Rb tumor suppressors (51, 52). We mapped the MDM2 domain (aa 1–200) required for the interaction between BAI1 and MDM2 and showed its functional implication in the regulation of PSD-95 stability, providing an explanation for destabilization of PSD-95 in *Bai1*$^{-/-}$ mice. In terms of the mechanism underlying the stabilization of PSD-95 in the presence of BAI1, we demonstrated that a direct association of BAI1 with PSD-95 is not required. Indeed, we showed that a BAI1 mutant with a deleted C-terminal PDZ-binding domain retained its stabilizing effect on PSD-95. This excludes a model in which BAI1 might directly compete with MDM2 for binding to PSD-95 or allosterically alter the ability of PSD-95 to bind MDM2. Instead, our data support a model in which BAI1 binds to MDM2 and alters its ability to promote PSD-95 ubiquitination and degradation. This model is supported by 3 distinct observations: (a) BAI1 cotransfection with MDM2 and PSD-95 in mammalian cells resulted in stabilization of PSD-95 protein and a dramatic decrease in PSD-95 ubiquitination; (b) cotransfection with a truncated MDM2 construct (aa 1–215) blocked the BAI1-MDM2 interaction and reversed the BAI1-mediated attenuation of PSD-95 ubiquitination; and (c) in *Bai1*$^{-/-}$ mice, the interaction between PSD-95 and MDM2 was found to be enhanced. Taken together, these findings suggest that BAI1 sequesters MDM2 and prevents it from binding to PSD-95.

Our studies show that BAI1 is an important component and regulator of the PSD. A recent study revealed that the human PSD contains over 1,000 proteins, and alterations in its function are associated with more than 100 distinct neurological and psychiatric diseases (53). However, the physiological roles played by most PSD components remain mysterious. Thus, our characterization of BAI1 as an important PSD regulator may provide a better understanding of the etiology of neurological diseases and identify novel diagnostic and therapeutic approaches. Autism spectrum disorder (ASD) is a neurodevelopmental disorder characterized by impaired social interactions, deficits in language acquisition, repetitive behaviors, and, in a subset of individuals, learning deficits (54). In mouse models of ASD, learning and memory deficits have been detected using the Morris water maze test (55, 56). The behavioral deficits observed in *Bai1*$^{-/-}$ mice, coupled with recent observations that perturbed synapse elimination in ASD may result from changes in the rate of proteasomal degradation of PSD-95 mediated by multiple autism-linked genes (57), open up the intriguing possibility that alterations in BAI1 function play a functional role in cognitive deficits associated with ASD. Additionally, the recent finding that *BAI1* is localized in a "hot spot" for de novo germline mutations in ASD patients (58), along with prior observations of a link between BAIAP2 and autism (59), is further suggestive of a potential connection between BAI1 and ASD pathology. One major finding of our study is that the deficits in adult *Bai1*$^{-/-}$ mice are reversible, as restoration of PSD-95 in adult *Bai1*$^{-/-}$ hippocampi was able to rescue synaptic plasticity deficits. These findings also provide a proof-of-principle demonstration that in patients suffering from decreased PSD-95 levels, as occurs in ASD, restoration of PSD-95 levels may have therapeutic implications, since the deficiency can still be restored in fully developed adult brains.

In summary, our findings demonstrate that BAI1 regulates synaptic plasticity in hippocampal CA1 neurons by antagonizing MDM2-mediated PSD-95 degradation, thereby revealing, for the first time to our knowledge, a physiological role of BAI1 in the brain. Our results identify BAI1 as a novel regulator of hippocampal synaptic plasticity and cognition that has wide-ranging implications for the understanding and possible treatment of a variety of neurological disorders.

Methods

Reagents and antibodies. The HEK 293FT cells (R700-07) were purchased from Invitrogen. PSD-95 antibody (2507), ubiquitin antibody (3936), HA-tagged antibody (3724), and GKAP antibody (13602) were purchased from Cell Signaling Technology. NMDAR1 antibody (2824-1), synaptophysin antibody (1870-1), and CaMKII antibody (2048-1) were from Epitomics. Actin antibody (sc-1616), tubulin antibody (sc-8035), Myc-tag (9E10) antibody (sc-40), and GFP antibody (sc-8334) were from Santa Cruz Biotechnology Inc. MDM2 antibody (M7815) was from Sigma-Aldrich; BAIAP2 antibody (ab37542) was from Abcam; and polyubiquitination-specific antibody FK1 clone (14219) was from Cayman Chemical. The BAI1 N-terminal antibody was described previously (13).

Generation of Bai1$^{-/-}$ *mice*. Homologous recombination was used to target the *Bai1* gene in ES cells. A 3.3-kb DNA fragment consisting of parts of intron 1 of the *Bai1* gene was used as the 5′ arm in the targeting construct. The 3′ arm consisted of a 3.4-kb genomic DNA fragment from intron 2. Exon 2 of the *Bai1* gene was replaced by a promoter-less β-gal cDNA (*LacZ*). A mini-neomycin resistance gene was also inserted between the 2 targeting arms. Following transfection of the 129S6/SvEvTac HZ2.2 ES cells (60) derived from 129/Sv mice (agouti coat color), clones were selected by G418. Clones (4 of 100) were identified as containing the homologous recombinant transgene by Southern blotting. Targeted ES cells with normal characteristics were used for injection into blastocysts from C57BL/6 mice (black coat color) and implanted into pseudo-pregnant females to generate chimeric mice. Mice with 90% or more agouti coat color were selected for further mating with C57BL/6 mice. For genotyping analysis, 3 primers were used for PCR. A sense primer in intron 1 of the *Bai1* gene (5′-CAGAGGAGCAGGTGGACAGAGAAAG-3′), 2 antisense primers, 1 in exon 2 of the *Bai1* gene (5′-TCAGGAGACAGTGGAAGCAGCG-3′) and the other in the *LacZ* gene (5′-TAACGCCAGGGTTTTCCCAGTCACG-3′) were used to simultaneously amplify both the WT (188 bp) and targeted (293 bp) alleles, respectively.

Quantification of brain vasculature. Assessment of the vascular area fraction was performed as previously described (61). The evaluator (G.N. Neigh) was blinded to the genotype of the animals. Vasculature was assessed using the stereological method of area fraction by counting the area of an overlaid grid occupied by blood vessels. Vessels were assessed in 1 hemisphere from every 12th section, beginning at the origin of the prefrontal cortex and concluding at the cerebellum. Three randomly selected fields per section were counted on 10 separate sections per mouse. The area fraction of blood vessels in the brain was compared between WT and KO mice (6 mice/group).

Animal behavior tests. An evaluator from the Emory Rodent Behavioral Core Facility blinded to the genotype of the animals performed all the tests under IACUC approval. The Morris water maze test was performed as described (62). Adult 4- to 6-month-old KO and WT litter-

mate mice were used. Acquisition training consisted of 4 trials per day for 5 days. Trials lasted 60 seconds or until the animal mounted the platform with a 15-minute inter-trial interval. A probe trial was conducted on day 6, wherein the platform was removed, the swim pattern for each animal was monitored, and the time spent in each quadrant was recorded and quantified. Statistics used were ANOVA and Dunnett's post-hoc test. For the marble-burying test, adult male mice were placed in a novel enclosure with 20 evenly spaced marbles. Mice were left undisturbed for 15 minutes, and then the number of buried marbles was counted. This test was conducted in the light cycle (7 mice/group). For the elevated plus maze, mice were placed in the center of the maze facing one of the open arms and allowed to freely explore the apparatus for 5 minutes, during which time their behavior was videotaped. Measures included the number of open-arm entries and time spent in open arms. For the light/dark test, mice were individually placed in the light side of the box, facing away from the dark compartment, and allowed to explore the apparatus for 5 minutes while being videotaped. Testing was performed under fluorescent lighting. Measures scored included latency to re-enter the light compartment and time spent in the light compartment.

Patch-clamp recording. Recording was performed as previously described (63). In summary, slices of 350 μm thickness containing the hippocampus were cut. Individual CA1 pyramidal cells positioned in the apical dendritic zone of the CA1 pyramidal layer were visualized in situ using differential interference contrast (DIC) microscopy. EPSCs on CA1 pyramidal cells were evoked by Schaffer collateral fiber stimulation. In all experiments, 50 μm picrotoxin was added to the patch solution to block $GABA_A$ currents exclusively in the recorded neuron. Slices were continuously perfused at 32°C with oxygenated artificial cerebrospinal fluid containing the $GABA_B$ receptor antagonist CGP36742 (5 μM). EPSCs (adjusted to 30% of maximal response) were evoked at 0.05 Hz, a 10-minute baseline period was recorded in each experiment, and recordings continued for at least 40 minutes after different stimulation protocols. Initial EPSC amplitudes were normalized to the average of the baseline EPSC amplitude. The membrane potential was held at –70 mV, except during HFS or different frequency stimulation protocols, when the potential was adjusted to –60 mV. To calculate the PPR, 2 EPSCs were evoked with interstimulus intervals of 20, 50, 100, and 200 ms. The PPR was calculated as (eEPSC2/eEPSC1), where eEPSC1 and eEPSC2 represent the amplitude of the first and the second eEPSC, respectively. To examine the basal synaptic transmission in CA1 pyramidal cells of WT and KO mice, 100 μm picrotoxin was added to the patch-recording solution to block $GABA_A$ receptor–mediated currents only in the recorded neuron. The membrane potential was held at –60 mV for all neurons. Spontaneous EPSCs were recorded in the presence of the selective $GABA_B$ receptor antagonist CGP36742 (2 μm). Spontaneous synaptic events were captured continuously for 30 seconds in both WT and KO mice. All events were detected offline and their amplitude and frequency calculated using Mini Analysis 6.0 software (Synaptosoft Inc.).

Quantification of dendritic spine morphology. During recordings, CA1 neurons were passively filled with biocytin (3%) contained in the patch-recording solution. After completion of LTP and LTD experiments, slices were fixed in paraformaldehyde (4%) overnight. Slices were then permeabilized with 0.5% Triton X-100, followed by incubation with a streptavidin-conjugated Alexa Fluor 594 antibody (Invitrogen). Images were acquired on a Leica DM-5500B microscope, and dendritic spine analysis was performed as described previously (64) by an observer (A.M. Swanson) blinded to the genotype of the samples.

Electron microscopic analysis. As described previously (65), PSD measurements were performed with ImageJ software (NIH) by an observer blinded to the genotype of the animals. Results are expressed as the mean ± SEM. SigmaPlot version 12.0 (Systat Software Inc.) was used for statistical analysis.

Hippocampal AAV injections. Six- to eight-week-old mice were anesthetized with ketamine and xylazine. The animals' heads were placed in a stereotactic apparatus (Stoelting). The bregma was identified, and a burr hole was made 1–1.5 mm laterally and 1.5–2 mm caudally. A 26-gauge Hamilton microsyringe was inserted to a depth of 1.5 mm, and 2 μl virus was injected into the hippocampus at a rate of 0.2 μl/minute. Incisions were closed and animals allowed to recover.

Primary granule neuron precursor culture. Cerebellar cells were purified as described previously (66). Briefly, cerebella from P5 WT mice were removed aseptically, cut into small pieces, and digested in 0.05% trypsin at 37°C for 5 minutes. DMEM plus 5% serum was added, and the tissue was then triturated using pipettes to obtain a single-cell suspension. The cell suspension was underlaid with a step gradient of 35% and 65% Percoll (Sigma-Aldrich) and centrifuged at high speed for 12 minutes at room temperature. Granule neuron precursors (GNPs) were harvested from the 35%–65% interface.

Statistics. The data were analyzed by 2-way ANOVA with Dunnett's post-hoc test and 2-tailed Student's *t* test. A *P* value of less than 0.05 was considered significant. All data represent the mean ± SEM. Further details can be found in Supplemental Table 2.

Study approval. All animal experiments were approved by the IACUC of Emory University.

Acknowledgments

We thank Helen Zhang of Emory University's Transgenic Mouse and Gene Targeting Core for help with generation of the *Bai1*$^{-/-}$ mouse line; Jason Schroeder and David Weinshenker of Emory University's Rodent Behavioral Core facility for help with the mouse behavior tests; and Xinping Huang of the Emory University Viral Vector Core for packaging the AAV. We thank Christine Blattner (Karlsruher Institut für Technologie, Karlsruhe, Germany) for the Myc-tagged MDM2 constructs. We thank Emily E. Hardy for help with the marble-burying test. This work was supported by grants from the NIH (CA86335, to E.G. Van Meir and CA138292, to the Winship Cancer Institute); the Southeastern Brain Tumor Foundation (to E.G. Van Meir); the CURE Childhood Cancer Foundation (to E.G. Van Meir); the St. Baldrick's Foundation (to E.G. Van Meir); the National Institute on Drug Abuse (NIDA) (T32 DA015040 and DA036316, to A.M. Swanson); and the National Institute of Neurological Disorders and Stroke (NINDS) and the Center for Neurodegenerative Disease (CND) (P30NS055077), in support of the Viral Vector and Microscopy Core facilities of Emory University. The spine analysis was performed using software provided by the NINDS/CND.

Address correspondence to: Erwin G. Van Meir, Department of Neurosurgery, Winship Cancer Institute, Emory University, 1365C Clifton Rd. N.E, C5078, Atlanta, Georgia 30322, USA. Phone: 404.778.5563; E-mail: evanmei@emory.edu

Shannon Matheny's present address is: Janssen Research and Development, Los Angeles, California, USA.

1. Martin SJ, Grimwood PD, Morris RG. Synaptic plasticity and memory: an evaluation of the hypothesis. *Annu Rev Neurosci*. 2000;23:649–711.
2. Neves G, Cooke SF, Bliss TV. Synaptic plasticity, memory and the hippocampus: a neural network approach to causality. *Nat Rev Neurosci*. 2008;9(1):65–75.
3. Bliss TV, Collingridge GL. A synaptic model of memory: long-term potentiation in the hippocampus. *Nature*. 1993;361(6407):31–39.
4. Malenka RC, Nicoll RA. Long-term potentiation — a decade of progress? *Science*. 1999;285(5435):1870–1874.
5. Chen C, Tonegawa S. Molecular genetic analysis of synaptic plasticity, activity-dependent neural development, learning, and memory in the mammalian brain. *Annu Rev Neurosci*. 1997;20:157–184.
6. Kim SJ, Linden DJ. Ubiquitous plasticity and memory storage. *Neuron*. 2007;56(4):582–592.
7. Citri A, Malenka RC. Synaptic plasticity: multiple forms, functions, and mechanisms. *Neuropsychopharmacology*. 2008;33(1):18–41.
8. Ho VM, Lee JA, Martin KC. The cell biology of synaptic plasticity. *Science*. 2011;334(6056):623–628.
9. Stephenson JR, Paavola KJ, Schaefer SA, Kaur B, Van Meir EG, Hall RA. Brain-specific angiogenesis inhibitor-1 signaling, regulation, and enrichment in the postsynaptic density. *J Biol Chem*. 2013;288(31):22248–22256.
10. Duman JG, et al. The adhesion-GPCR BAI1 regulates synaptogenesis by controlling the recruitment of the Par3/Tiam1 polarity complex to synaptic sites. *J Neurosci*. 2013;33(16):6964–6978.
11. Paavola KJ, Hall RA. Adhesion G protein-coupled receptors: signaling, pharmacology, and mechanisms of activation. *Mol Pharmacol*. 2012;82(5):777–783.
12. Nishimori H, et al. A novel brain-specific p53-target gene, BAI1, containing thrombospondin type 1 repeats inhibits experimental angiogenesis. *Oncogene*. 1997;15(18):2145–2150.
13. Kaur B, Brat DJ, Calkins CC, Van Meir EG. Brain angiogenesis inhibitor 1 is differentially expressed in normal brain and glioblastoma independently of p53 expression. *Am J Pathol*. 2003;162(1):19–27.
14. Zhu D, Hunter SB, Vertino PM, Van Meir EG. Overexpression of MBD2 in glioblastoma maintains epigenetic silencing and inhibits the antiangiogenic function of the tumor suppressor gene BAI1. *Cancer Res*. 2011;71(17):5859–5870.
15. Ozkan A, et al. Temporal expression analysis of angiogenesis-related genes in brain development. *Vasc Cell*. 2012;4(1):16.
16. Cork SM, et al. A proprotein convertase/MMP-14 proteolytic cascade releases a novel 40 kDa vasculostatin from tumor suppressor BAI1. *Oncogene*. 2012;31(50):5144–5152.
17. Kaur B, et al. Vasculostatin inhibits intracranial glioma growth and negatively regulates in vivo angiogenesis through a CD36-dependent mechanism. *Cancer Res*. 2009;69(3):1212–1220.
18. Kaur B, Brat DJ, Devi NS, Van Meir EG. Vasculostatin, a proteolytic fragment of brain angiogenesis inhibitor 1, is an antiangiogenic and antitumorigenic factor. *Oncogene*. 2005;24(22):3632–3642.
19. Cork SM, Van Meir EG. Emerging roles for the BAI1 protein family in the regulation of phagocytosis, synaptogenesis, neurovasculature, and tumor development. *J Mol Med (Berl)*. 2011;89(8):743–752.
20. Klenotic PA, et al. Histidine-rich glycoprotein modulates the anti-angiogenic effects of vasculostatin. *Am J Pathol*. 2010;176(4):2039–2050.
21. Park D, et al. BAI1 is an engulfment receptor for apoptotic cells upstream of the ELMO/Dock180/Rac module. *Nature*. 2007;450(7168):430–434.
22. Hochreiter-Hufford AE, et al. Phosphatidylserine receptor BAI1 and apoptotic cells as new promoters of myoblast fusion. *Nature*. 2013;497(7448):263–267.
23. Valen E, et al. Genome-wide detection and analysis of hippocampus core promoters using DeepCAGE. *Genome Res*. 2009;19(2):255–265.
24. Morris R. Developments of a water-maze procedure for studying spatial learning in the rat. *J Neurosci Methods*. 1984;11(1):47–60.
25. Tsien JZ, Huerta PT, Tonegawa S. The essential role of hippocampal CA1 NMDA receptor-dependent synaptic plasticity in spatial memory. *Cell*. 1996;87(7):1327–1338.
26. Yuste R, Bonhoeffer T. Morphological changes in dendritic spines associated with long-term synaptic plasticity. *Annu Rev Neurosci*. 2001;24:1071–1089.
27. Harris KM, Jensen FE, Tsao B. Three-dimensional structure of dendritic spines and synapses in rat hippocampus (CA1) at postnatal day 15 and adult ages: implications for the maturation of synaptic physiology and long-term potentiation. *J Neurosci*. 1992;12(7):2685–2705.
28. Scannevin RH, Huganir RL. Postsynaptic organization and regulation of excitatory synapses. *Nat Rev Neurosci*. 2000;1(2):133–141.
29. Sheng M, Kim E. The postsynaptic organization of synapses. *Cold Spring Harb Perspect Biol*. 2011;3(12):a005678.
30. Cheng D, et al. Relative and absolute quantification of postsynaptic density proteome isolated from rat forebrain and cerebellum. *Mol Cell Proteomics*. 2006;5(6):1158–1170.
31. El-Husseini AE, Schnell E, Chetkovich DM, Nicoll RA, Bredt DS. PSD-95 involvement in maturation of excitatory synapses. *Science*. 2000;290(5495):1364–1368.
32. Ehrlich I, Klein M, Rumpel S, Malinow R. PSD-95 is required for activity-driven synapse stabilization. *Proc Natl Acad Sci U S A*. 2007;104(10):4176–4181.
33. Chen X, et al. PSD-95 is required to sustain the molecular organization of the postsynaptic density. *J Neurosci*. 2011;31(17):6329–6338.
34. Colledge M, et al. Ubiquitination regulates PSD-95 degradation and AMPA receptor surface expression. *Neuron*. 2003;40(3):595–607.
35. Kulikov R, Winter M, Blattner C. Binding of p53 to the central domain of Mdm2 is regulated by phosphorylation. *J Biol Chem*. 2006;281(39):28575–28583.
36. Kim E, et al. GKAP, a novel synaptic protein that interacts with the guanylate kinase-like domain of the PSD-95/SAP90 family of channel clustering molecules. *J Cell Biol*. 1997;136(3):669–678.
37. Hung AY, Sung CC, Brito IL, Sheng M. Degradation of postsynaptic scaffold GKAP and regulation of dendritic spine morphology by the TRIM3 ubiquitin ligase in rat hippocampal neurons. *PLoS One*. 2010;5(3):e9842.
38. Szymczak AL, et al. Correction of multi-gene deficiency in vivo using a single 'self-cleaving' 2A peptide-based retroviral vector. *Nat Biotechnol*. 2004;22(5):589–594.
39. Topinka JR, Bredt DS. N-terminal palmitoylation of PSD-95 regulates association with cell membranes and interaction with K+ channel Kv1.4. *Neuron*. 1998;20(1):125–134.
40. Fukata M, Fukata Y, Adesnik H, Nicoll RA, Bredt DS. Identification of PSD-95 palmitoylating enzymes. *Neuron*. 2004;44(6):987–996.
41. Park D, Ravichandran KS. Emerging roles of brain-specific angiogenesis inhibitor 1. *Adv Exp Med Biol*. 2010;706:167–178.
42. Mori K, et al. Brain-specific angiogenesis inhibitor 1 (BAI1) is expressed in human cerebral neuronal cells. *Neurosci Res*. 2002;43(1):69–74.
43. Whitlock JR, Heynen AJ, Shuler MG, Bear MF. Learning induces long-term potentiation in the hippocampus. *Science*. 2006;313(5790):1093–1097.
44. Migaud M, et al. Enhanced long-term potentiation and impaired learning in mice with mutant postsynaptic density-95 protein. *Nature*. 1998;396(6710):433–439.
45. Kemp A, Manahan-Vaughan D. Hippocampal long-term depression: master or minion in declarative memory processes? *Trends Neurosci*. 2007;30(3):111–118.
46. Kim MH, et al. Enhanced NMDA receptor-mediated synaptic transmission, enhanced long-term potentiation, and impaired learning and memory in mice lacking IRSp53. *J Neurosci*. 2009;29(5):1586–1595.
47. Sawallisch C, et al. The insulin receptor substrate of 53 kDa (IRSp53) limits hippocampal synaptic plasticity. *J Biol Chem*. 2009;284(14):9225–9236.
48. Luscher C, Nicoll RA, Malenka RC, Muller D. Synaptic plasticity and dynamic modulation of the postsynaptic membrane. *Nat Neurosci*. 2000;3(6):545–550.
49. Beique JC, Lin DT, Kang MG, Aizawa H, Takamiya K, Huganir RL. Synapse-specific regulation of AMPA receptor function by PSD-95. *Proc Natl Acad Sci U S A*. 2006;103(51):19535–19540.
50. Carlisle HJ, Fink AE, Grant SG, O'Dell TJ. Opposing effects of PSD-93 and PSD-95 on long-term potentiation and spike timing-dependent plasticity. *J Physiol*. 2008;586(Pt 24):5885–5900.
51. Haupt Y, Maya R, Kazaz A, Oren M. Mdm2 promotes the rapid degradation of p53. *Nature*. 1997;387(6630):296–299.
52. Fåhraeus R, Olivares-Illana V. MDM2's social network. *Oncogene*. 2014;33(35):4365–4376.
53. Bayes A, et al. Characterization of the proteome, diseases and evolution of the human postsynaptic density. *Nat Neurosci*. 2011;14(1):19–21.
54. Geschwind DH, Levitt P. Autism spectrum disorders: developmental disconnection syndromes. *Curr Opin Neurobiol*. 2007;17(1):103–111.
55. Silverman JL, Yang M, Lord C, Crawley JN. Behavioural phenotyping assays for mouse models of autism. *Nat Rev Neurosci*. 2010;11(7):490–502.
56. Crawley JN. Designing mouse behavioral tasks relevant to autistic-like behaviors. *Ment Retard Dev Disabil Res Rev*. 2004;10(4):248–258.
57. Tsai NP, et al. Multiple autism-linked genes

mediate synapse elimination via proteasomal degradation of a synaptic scaffold PSD-95. *Cell*. 2012;151(7):1581–1594.
58. Michaelson JJ, et al. Whole-genome sequencing in autism identifies hot spots for de novo germline mutation. *Cell*. 2012;151(7):1431–1442.
59. Toma C, et al. Association study of six candidate genes asymmetrically expressed in the two cerebral hemispheres suggests the involvement of BAIAP2 in autism. *J Psychiatr Res*. 2011;45(2):280–282.
60. Lee Z, et al. Role of LPA4/p2y9/GPR23 in negative regulation of cell motility. *Mol Biol Cell*. 2008;19(12):5435–5445.
61. Neigh GN, Owens MJ, Taylor WR, Nemeroff CB. Changes in the vascular area fraction of the hippocampus and amygdala are induced by prenatal dexamethasone and/or adult stress. *J Cereb Blood Flow Metab*. 2010;30(6):1100–1104.
62. Lee SE, et al. RGS14 is a natural suppressor of both synaptic plasticity in CA2 neurons and hippocampal-based learning and memory. *Proc Natl Acad Sci U S A*. 2010;107(39):16994–16998.
63. Li C, Dabrowska J, Hazra R, Rainnie DG. Synergistic activation of dopamine D1 and TrkB receptors mediate gain control of synaptic plasticity in the basolateral amygdala. *PLoS One*. 2011;6(10):e26065.
64. Gourley SL, Swanson AM, Koleske AJ. Corticosteroid-induced neural remodeling predicts behavioral vulnerability and resilience. *J Neurosci*. 2013;33(7):3107–3112.
65. Villalba RM, Smith Y. Differential structural plasticity of corticostriatal and thalamostriatal axospinous synapses in MPTP-treated Parkinsonian monkeys. *J Comp Neurol*. 2011;519(5):989–1005.
66. Wechsler-Reya RJ, Scott MP. Control of neuronal precursor proliferation in the cerebellum by Sonic Hedgehog. *Neuron*. 1999;22(1):103–114.